Solar Physics
DOI: 10.1007/•••••-•••-•••-••••-•

Simulations of 3D Magnetic Merging: Resistive Scalings for Null Point and QSL Reconnection

Frederic Effenberger[1,2] **and I. J. D. Craig**[1]

© Springer ••••

arXiv:1601.02044v1 [astro-ph.SR] 8 Jan 2016

Abstract Starting from an exact, steady-state, force-free solution of the magnetohydrodynamic (MHD) equations, we investigate how resistive current layers are induced by perturbing line-tied three-dimensional magnetic equilibria. This is achieved by the superposition of a weak perturbation field in the domain, in contrast to studies where the boundary is driven by slow motions, like those present in photospheric active regions. Our aim is to quantify how the current structures are altered by the contribution of so called quasi-separatrix layers (QSLs) as the null point is shifted outside the computational domain. Previous studies based on magneto-frictional relaxation have indicated that, despite the severe field line gradients of the QSL, the presence of a null is vital in maintaining fast reconnection. Here, we explore this notion using highly resolved simulations of the full MHD evolution. We show that for the null-point configuration, the resistive scaling of the peak current density is close to $J \sim \eta^{-1}$, while the scaling is much weaker, *i.e.* $J \sim \eta^{-0.4}$, when only the QSL connectivity gradients provide a site for the current accumulation.

Keywords: Magnetic reconnection; Electric currents and current sheets; Flares; Magnetic fields, models; Magnetic fields, corona

1. Introduction

The development of current singularities in a three-dimensional magnetohydrodynamic (MHD) plasma evolution is an active topic in coronal astrophysics with high relevance to the general problem of magnetic reconnection (Priest and Forbes, 2000) and related particle acceleration mechanisms (*e.g.* Heerikhuisen, Litvinenko, and Craig, 2002; Stanier, Browning, and Dalla, 2012). In particular, if reconnection is to be effective in altering the magnetic topology, very strong localized currents must be present in the vicinity of the reconnection site. If these conditions on the current density are not met, the weak coronal resistivity can strongly inhibit the reconnection rate.

[1] Department of Mathematics, University of Waikato,
Private Bag 3105, Hamilton, New Zealand
[2] Department of Physics and KIPAC, Stanford University,
Stanford, CA 94305, USA, feffen@stanford.edu

In the past, models of two-dimensional (2D) reconnection have yielded much insight into the formation of near singular current sheets, as supported by 2D MHD simulations (*e.g.* Biskamp, 1986) and analytic modeling (*e.g.* Forbes, 1982). Although the three-dimensional merging problem has been less intensively explored, it is known that 3D merging may involve not only current sheets, as in "fan" reconnection, but also the quasi-cylindrical current tubes of "spine" reconnection (*e.g.* Craig and Fabling, 1996). A further form, "separator" reconnection, involves thin current ribbons that form along field lines linking any two nulls (Heerikhuisen and Craig, 2004). Longcope (2005) gives a review on the topological aspects of three-dimensional reconnection. These topological forms derive from the 3D eigenstructure of the null and cannot be adequately represented in simplified planar geometries.

We are also concerned with reconnection that occurs in the absence of a null. The key entity in this case is the geometry of the quasi-separatrix layers (QSLs), which provide a region of rapid variation in the field line connectivity (Demoulin *et al.*, 1996; Priest and Titov, 1996; Galsgaard, 2000; Aulanier *et al.*, 2006; Baker *et al.*, 2009). This behaviour can be quantified in terms of the squashing factors of the configuration (Titov, 2007), which give a measure of the connectivity gradient. Notably, MHD simulations of line-tied QSL configurations suggest that, by systematically decreasing the resistivity, current accumulation and the collapse to small length scales may be unbounded (Aulanier, Pariat, and Démoulin, 2005; Effenberger *et al.*, 2011).

A related problem was tackled by Craig and Effenberger (2014, hereafter Paper I). There, a non-resistive, Lagrangian magneto-frictional relaxation method (Craig and Sneyd, 1986; Pontin *et al.*, 2009; Craig and Pontin, 2014) was used to obtain a near singular relaxed configuration. It was found that the divergent scaling of the QSL current could be significantly accelerated by the presence of a magnetic null within the computational domain. QSL diagnostics have also been used in related contexts, for example in studies on tearing modes with particle in cell methods (Finn *et al.*, 2014) or reduced MHD models of flux tube reconnection in solar coronal loops (Milano *et al.*, 1999).

The goal of the present study is to extend Paper I by performing *resistive* three-dimensional MHD simulations with the finite volume code PLUTO (Mignone *et al.*, 2007) to quantify the resistive scalings of the simulated current layer. In common with Paper I, we show how the current build up is altered by shifting the position of a magnetic null in the computational domain. To support our results, we first summarize in Section 2 theoretical arguments for different resistive scalings. We then describe our field setup in Section 3 before presenting our results and conclusion in the last two sections. Details on the numerical implementation are given in the Appendix.

2. Theoretical Arguments for Resistive Scalings

Magnetic reconnection studies often assume a steady state description based on an "open" geometry in which plasma, continuously washed into the current layer, is ejected by the reconnection exhaust. This approach generally leads to

slow reconnection rates—Sweet-Parker scalings possibly enhanced by flux pile-up factors—no matter whether 2D or 3D geometries are considered (Craig and Fabling, 1996). An alternative method is to examine the dynamic collapse of "closed" line-tied X-points, which are subject to an initial, topology-altering disturbance. In these models cold plasma is contained within a highly conducting, rigid boundary across which there is no mass flow. Under these conditions the reconnection rate ηJ can be fast—effectively independent of the plasma resistivity η. This scaling contrasts markedly with the relatively weak build-up of current J in Sweet-Parker merging $\eta J \sim \eta^{1/2}$.

Although the study of 3D X-point geometries is an active research area, we know of no analytic argument that predicts the reconnection rate associated with collapsing, 3D compressible X-points. A linearized treatment is provided by Rickard and Titov (1996), but most studies rely on extrapolating numerical results, obtained for computationally accessible resistivities (typically $10^{-4} < \eta < 10^{-2}$), down to physically plausible values $\eta \lesssim 10^{-9}$. Note that in the non-dimensional units we employ (see below) the Alfvén crossing time of the system is of of order unity and η is an inverse Lundquist number.

One possibility for gaining insight into 3D reconnection scalings is to examine the non-linear behaviour of planar X-point models under the idealisation $\partial/\partial z = 0$ but in the presence of an axial "guide" field $b\,\hat{\mathbf{z}}$. The common ground between 2D and 3D X-point collapse models (*e.g.* Pontin and Craig, 2005) also suggests that it is worthwhile revisiting the non-linear $2\frac{1}{2}$D collapse problem.

2.1. Planar X-point collapse, Y-point scaling

We consider a planar potential field, immersed in a uniform background plasma. As in Paper I, we assume that length scales, densities and magnetic field intensities are scaled with respect to typical coronal values. Since we assume the gas pressure term to be negligible, all wave motions are purely Alfvénic. All velocities are expressed in units of the reference Alfvén speed $v_{\rm A}$. Time is measured in units of the global length scale divided by $v_{\rm A}$.

The initial field can then be written

$$\mathbf{B}_{\rm E} = \nabla\psi_{\rm E} \times \hat{\mathbf{z}} + b\,\hat{\mathbf{z}} \tag{1}$$

where $b\hat{\mathbf{z}}$ is constant and

$$\psi_{\rm E} = \frac{1}{2}(y^2 - x^2) = -\frac{r^2}{2}\cos(2\phi) \tag{2}$$

is the equilibrium flux function. For the moment we assume the axial field is turned off, so $b = 0$.

The equilibrium field is line-tied on the outer boundary $r = 1$ and subject to an initial radial wave disturbance $\psi = \psi(r)$. This launches an azimuthal disturbance field $B_\phi = \partial\psi/\partial r$ in the form of a cylindrical wave that propagates inwards from the outer boundary $r = 1$. The imploding wave continually steepens due to the gradient in the Alfvén speed $v_{\rm A} \propto r$. However, a point $r = R$ (say) is reached where the disturbance field begins to overwhelm the background field.

Cylindrical symmetry is then lost as the X-point field is weakened or reinforced in adjacent lobes. The disturbance field now becomes increasingly one-dimensional $B_\phi \to B_\mathrm{s}$ and, in the absence of resistivity, a Y-type, finite time singularity emerges. For finite η, however, a resistive length scale Δ is introduced that allows the wave speed $B_\mathrm{s}/\sqrt{\rho}$ to be matched by the diffusion speed η/Δ. In this case, by neglecting the relatively weak density dependence of the wave speed, we obtain (McClymont and Craig, 1996)

$$\Delta \sim \eta, \quad R \sim B_\mathrm{s} \sim \eta^0, \quad J \sim \eta^{-1}. \tag{3}$$

These resistive scalings define the thickness, length, field strength and current density of the Y-point field. Note that the length $R \gg \Delta$ of the current sheet is determined by the radius at which cylindrical symmetry is lost and generally lies well outside the diffusion layer of thickness η.

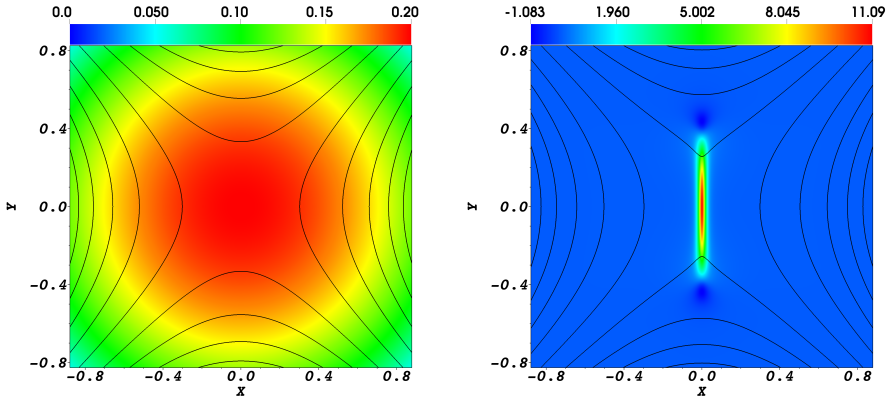

Figure 1. Illustration of the two-dimensional Y-point current formation and field line structure. The color coding gives the J_z current while the black lines show field lines, integrated from the boundary. The left panel shows the initial condition at $t = 0$, while the right panel is a snapshot at $t = 2$ (Alfvén times). The run was performed on a grid of 400×400 points with $\eta = 3 \times 10^{-3}$.

To illustrate the topology and current formation process of the previous discussion, we performed a simple two-dimensional, line-tied simulation of the X-point field of Equation (1) with perturbation $\psi_\mathrm{p} = A(1 - x^2)(1 - y^2)$. In this case we find that $A = 0.05$ is sufficient to provide a current layer of global length consistent with the scalings of Equation (3) and the non-linearity condition $R \gg \Delta$.

Here, we only present two snapshots of the evolution in Figure 1. While initially, the configuration is nearly symmetric, at a later stage, due to the perturbation and the corresponding change in topology, the current collapses to a nearly one-dimensional structure and the magnetic field lines adapt to the Y-point geometry around the endpoints of the current sheet. Reduction of the resistivity leads to correspondingly larger current densities and smaller perpendicular length scales of the sheet. The perturbation amplitude A determines mainly the length of the current sheet, but, within limits set by the global geometry, does not influence resistive scalings for the peak current density and

current sheet thickness. We do not pursue the investigation of this 2D configuration further at this point, since this has already been done extensively in previous studies (*e.g.*, Priest and Forbes, 2000, and references therein). More details on the linear and non-linear treatment of X-point plasmas can be found for example in Craig and McClymont (1993).

The scalings of Equation (3) are based on an analysis given by McClymont and Craig (1996). These authors point out that these results are in good agreement with dynamic simulations of resistive current layers as well as the formally exact, non-linear imploding field models of Forbes (1982), which yield $\Delta \sim \eta^{0.892}$ and $J \sim \eta^{-1.04}$. Even so, the fast reconnection rate is expected to stall when significant back pressures due to strong axial fields oppose the localization.

2.2. Arguments for QSL Scalings

Suppose now that the axial field is no longer vanishing. The null point is removed but the axial field is compressed by the implosion leading to back pressures which oppose the localization. McClymont and Craig (1996) show that the fast scaling can persist only if

$$\frac{1}{2}b^2 \leq \eta. \tag{4}$$

When this condition is not met the reconnection rate can become very slow, approaching the static limit $\eta J \sim \eta$.

We are primarily interested in how these results impact on 3D nulls in the presence of QSLs. Clearly, insofar as QSL structures can be represented by X-points threaded by axial fields, they cannot be expected to provide fast reconnection, at least for realistic amplitudes b. In the case of fully 3D line-tied configurations, however, the presence of a null at some point within the source volume should act to focus and intensify the current. This tendency could be reinforced by the strong squashing factors that characterize the QSL configuration. Our expectation, therefore, is that while the reconnection rate associated with strong QSLs is probably slow, it can be significantly accelerated if a null point is located in the vicinity of the QSL. This reasoning is explored computationally in the analysis that follows.

3. Potential Field Formulation

We base our analysis on the potential field model of Paper I [Equation (9)], which has the general form

$$\mathbf{P} = [x, (\mu - 1)y, -\mu z + b]\,. \tag{5}$$

The field is defined within the cubic domain $x, y, z = \pm 1$, and line-tied on the bounding surfaces. Note that although $\mu = 0$ allows X-point fields typified by Equation (1) to be modelled, we now have line-tied boundary conditions at $z = \pm 1$. More generally, μ can be regarded as a proxy for the field asymmetry, which we fix at -0.4 in the present study. The parameter b is more significant

since it allows a continuously shift of the magnetic null along the $z-$axis. The null is located at the point $\mathbf{r}_0 = (0, 0, b/\mu)$ and, by adjusting b, the null can be transferred outside the computational domain. Thus, we find nulls located at $z_0 = -0.75$ and $z_0 = -1.25$, corresponding to the respective choices $b = 0.3$ and $b = 0.5$. The first case provides a convenient platform for null point reconnection to be modelled. However, by taking $b = 0.5$ the null "disappears" while the QSL geometry is retained, potentially altering the reconnection rate. We note that the type of potential field considered here can be regarded as an approximation to a more general force free field; see the discussion in Paper I.

To initiate the current formation, a suitable perturbation of the equilibrium field $\mathbf{P}$ is required. The combined initial field configuration is then given by $\mathbf{B}_0 = \mathbf{P} + \mathbf{B}_\mathrm{p}$ and we assume the initial velocity field to vanish. For comparison with Paper I, we adopt the same type of perturbation field, with amplitude $A = 0.3$:

$$\mathbf{B}_\mathrm{p} = [A \sin(\pi x/2) \cdot (1 - y^2) \cdot (1 - z^2) \cdot \exp(-4x^2 - 3y^2)]\hat{\mathbf{y}}\,. \tag{6}$$

In the vicinity of the origin this perturbation reduces to the form $\mathbf{B}_\mathrm{p} \propto (0, x, 0)$. As shown in Paper I, when added to the the X-point field of Equation (5), the effect is to tilt the spine and drive implosive currents within the fan. The global perturbation also contains additional exponential factors whose role is to constrain initial currents and forces in the outer field to be of order unity. Their slightly different strengths are chosen to break any artificial symmetries imposed by the perturbation. Further discussion on the form of the perturbation can also be found in Section 2.6 of Craig and Pontin (2014). Details of the numerical setup which is used to solve the field evolution are given in the Appendix.

It should be stressed that the role of the idealised global perturbation is solely to initiate a collapse towards a resistive current layer. For actual coronal fields, the perturbation is probably supplied by photospheric motions during a slow build-up phase, while we impose the perturbation directly with the initial field in the domain. Other studies (Galsgaard, 2000; Aulanier, Pariat, and Démoulin, 2005; Effenberger *et al.*, 2011) include such motions by suitable velocity fields at the boundaries. To retain the direct comparability with our previous results from Paper I and to keep the run times for individual simulations relatively short, we stick with this kind of direct perturbation field. The small divergences of the magnetic field introduced by this particular form of perturbation —or more generally through discretisation errors in the code— were not relevant in the study of Paper I since the Lagrangian scheme is solenoidal by construction. In the present study, the smallness of the perturbation and the divergence cleaning method keep the divergence error low. The scaling results discussed in the next section should not depend on the actual form chosen for the perturbation and its amplitude (*cf.* the previous discussion on the planar X-point collapse).

4. Current Structure, Time Evolution, and Scaling Results

We performed runs of the two field configurations described in the previous section ($b = 0.3$ and $b = 0.5$) for different values of η, between 10^{-2} and 10^{-4}.

Since previous analytic and numerical studies have confirmed that the properties of the current layer at peak current (Heerikhuisen and Craig, 2004) provide a reliable guide to the reconnection rate, we follow the magnetic field evolution until maximum current density is achieved.

For larger resistivities, the problem is too diffusive to allow for a sufficiently strong current localization, so we disregard results from such runs. Similarly, resistivities smaller than 10^{-4} turn out to be computationally unfeasible, since even at the highest transverse resolution in the current sheet region of $\Delta = 5\times10^{-4}$ (*cf.* the description of the numerical grid in the appendix) the numerical dissipation will start to dominate the evolution.

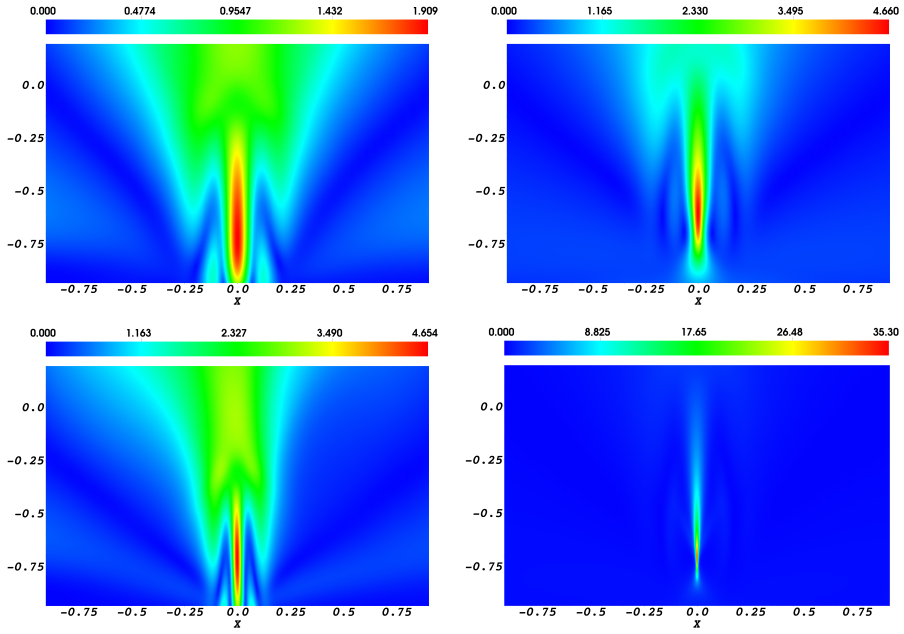

Figure 2. Current sheet structure around the time of peak current density in the x-z-plane ($y = 0$); the color coding gives the current density. The left column shows results for the QSL only configuration ($b = 0.5$) while the right column shows the configuration with a null at -0.75 ($b = 0.3$). The top row has a value for the resistivity of $\eta = 10^{-3}$ and the bottom row $\eta = 10^{-4}$.

Figure 2 shows the structure of the accumulated current in a planar cut at $y = 0$ around the time of peak current density. The left column gives results for the QSL-only configuration ($b = 0.5$) and the right column shows the current structure when a null is present at $z = -0.75$ ($b = 0.3$). The strong localization provided by the null is clearly a dominant feature, while the current remains more broadly distributed without the null. The collapse to much smaller length scales for respectively smaller resistivities is evident, and highlights the need for sufficient grid resolution.

The time evolution of the current build-up in the null-point case is given in Figure 3, for four different resistivities. As expected, the build-up takes longer for

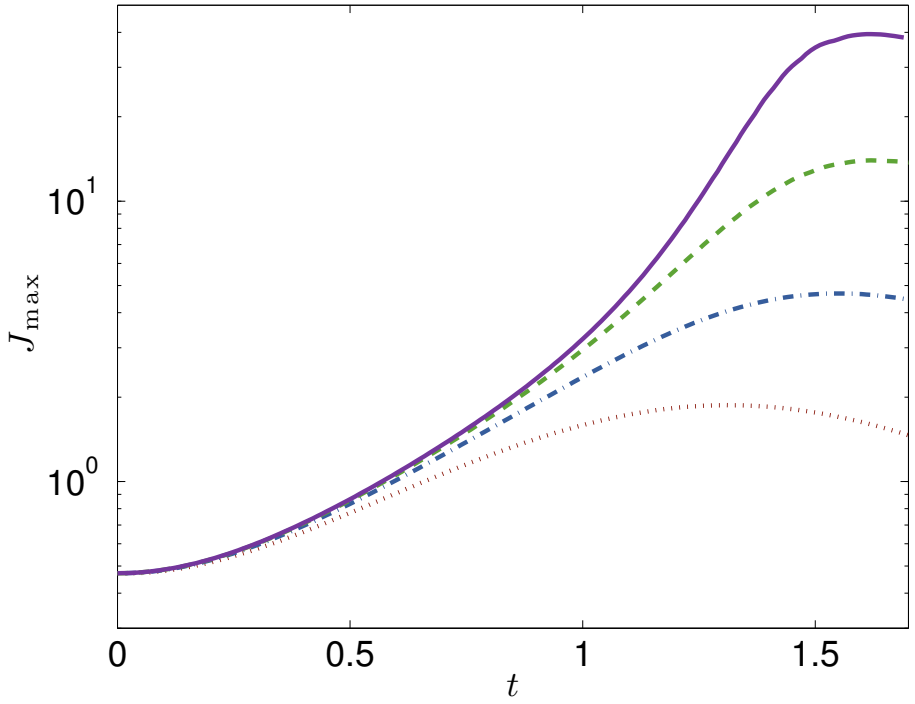

Figure 3. Time evolution of the maximum current build up in the central current sheet region in the magnetic null case ($b = 0.3$) for four different resistivities, $\eta = 3 \times 10^{-3}$ (red, dotted), $\eta = 10^{-3}$ (blue, dot-dashed), $\eta = 3 \times 10^{-4}$ (green, dashed), and $\eta = 10^{-4}$ (purple, solid).

the more intense localizations associated with the weaker resistivities. Specifically, the maximum current density peaks at about 1.5 Alfvén times for low resistivities, while for higher values, the evolution is broader and less pronounced. It appears that a distinct fast phase of current accumulation is only present for small resistivities, hinting at a self-maintained sheet collapse, which is inhibited at too large η. Presumably this is why resistive current layers at sufficiently small resistivities very closely resemble the near-singular, force-free, current structures that derive from the magneto-frictional relaxation of Paper I.

Figure 4 summarizes the main scaling results of our study. Blue crosses indicate the peak current densities for runs with different resistivities when the null is in the domain, while the red + symbols give the results for QSL only currents. We see a clearly different trend in the scaling of maximum current with resistivity. While the best-fit slope (dashed lines) is close to a theoretical η^{-1} scaling (see the discussion in Section 2) when the null-point lies in the domain, the scaling is much weaker, tending towards a weak scaling between $\eta^{-0.5}$ and $\eta^{-0.25}$, when only the QSL structure is present. Note that the lower bound of $\eta^{-0.25}$ follows from the Lagrangian results of Paper I, where a scaling exponent of about 0.5 for the current accumulation with resolution was found. This converts to an Eulerian exponent of 0.25 in a strictly one-dimensional setting (see the discussion in the appendix of Craig and Litvinenko, 2005). In a three-dimensional configuration, however, there is no exact equivalence between

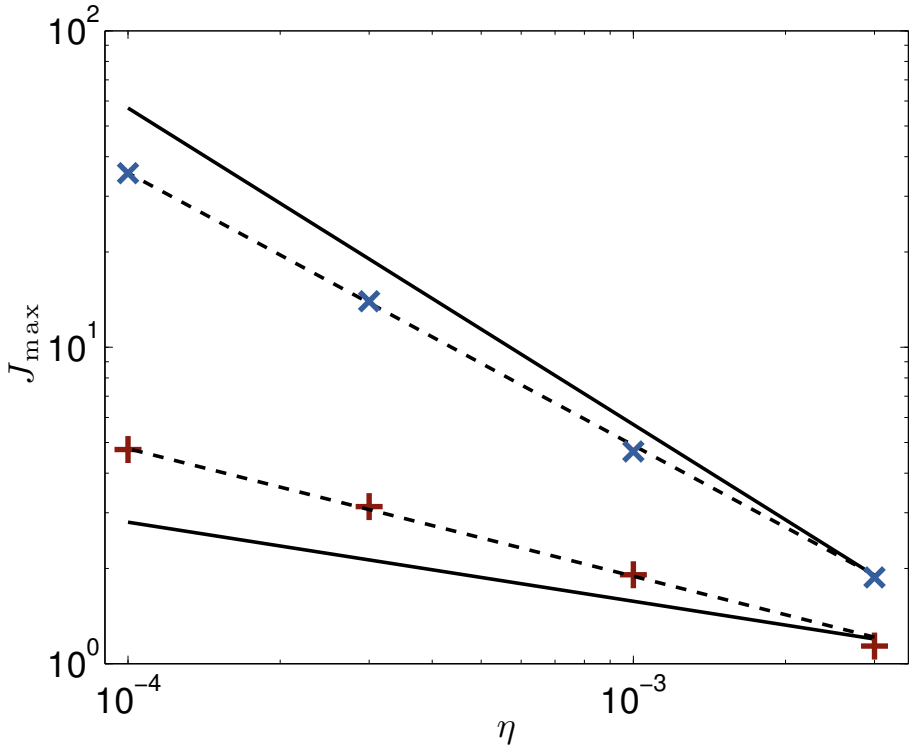

Figure 4. Resistive scalings of the peak current density for $b = 0.3$ (blue, x), *i.e.* the magnetic null in the domain, and $b = 0.5$ (red, +), *i.e.* only the QSL structure present. The dashed lines give the best-fit power laws ($J \sim \eta^\gamma$) with exponents $\gamma = -0.86$ and $\gamma = -0.40$, respectively. The solid lines represent theoretical limiting cases of a $\gamma = -1$ and $\gamma = -0.25$ scaling, to guide the eye.

the Lagrangian and Eulerian description, so this can only be regarded as a rough lower bound. The results corroborate the earlier findings of Paper I, in that there is a qualitatively different current accumulation behavior, induced by the three-dimensional magnetic null. We emphasize, however, that we see no signs of saturation of current concentration in either case, for the considered range of resistivities.

An interesting feature of the above results is the extent to which they differ from a $2\frac{1}{2}$D description, based on a planar, line-tied X-point threaded by a uniform axial field. As indicated by Equation (4), and confirmed by numerical studies, fast reconnection is easily stalled by the back pressure introduced by the compression of $b\,\hat{\mathbf{z}}$. This problem is worsened when line-tying on the upper and lower planes $z = \pm 1$ is introduced, because tension of the axial field can come into play. In this case, modest axial fields can prevent the X-point implosion (Craig and Pontin, 2014). Only by reducing the initial $b\,\hat{\mathbf{z}}$ amplitude, or extending the distance between the z-boundaries, can the collapse be recovered. Clearly, the presence of a null negates these difficulties.

Finally, we should mention that although gas pressure is negligible in all our simulations, the extreme scalings required to maintain fast reconnection are likely to remain sensitive to finite β effects (Pontin, Bhattacharjee, and Galsgaard, 2007). Since coronal plasmas are low β, however, the principle features of X-point collapse should not be undone.

5. Summary and Conclusion

We have studied the implosive collapse of a line-tied 3D X-point and QSL configuration, using a resistive MHD code. Our results, evaluated at the time of peak current density, directly compare resistive scalings for perturbed QSL and null-point initial equilibrium fields. The implication is that, while QSL equilibria lead to divergent current structures in the limit of small η, the reconnection rate is considerably enhanced by the presence of a null within the computational domain. Notably, for moderate finite amplitude disturbances, the merging rate can approach the fast scaling $J \sim \eta^{-1}$ over the range of resistivities considered. In contrast, the QSL scalings, though still divergent, are significantly weaker, *i.e.* about $J \sim \eta^{-0.4}$.

It is interesting that the present results provide a direct extension of the results provided by the Lagrangian magneto-frictional method of Paper I. In the Lagrangian approach, $\nabla \cdot \mathbf{B}$ is guaranteed to vanish and flux conservation is automatically satisfied. The proper time evolution is not accessible, however, and results have to be extracted from the near-singular, force free-field that emerges during the late stages of the evolution. That the methods of Paper I and the resistive MHD approach provide a consistent physical interpretation goes some way, we believe, in establishing the veracity of the present results. It will be of interest therefore, to explore these findings using additional parallel computing capacities to improve the numerical resolution and extend the parameter range of the simulations. An extension to different cases of boundary conditions and perturbations by boundary driving should yield new insights on the general applicability of our findings to different solar flare scenarios.

Acknowledgements We acknowledge the work that has been devoted to the development and documentation of the PLUTO MHD code used in this study. Work performed by F.E. was partially supported by NASA grant NNX14AG03G. Constructive comments of an anonymous referee are appreciated.

Appendix

A. Code Setup

We evolve the perturbed field of Section 3 according to the full set of non-relativistic MHD equations, using the finite volume code PLUTO (version 4.1, see http://plutocode.ph.unito.it). The code manual and the foundational papers of the code (Mignone *et al.*, 2007, 2012) describe tests and the fundamental capabilities and solution methods available in the code. Here, we only briefly describe the setup choices and configuration we use for our particular problem.

The ideal MHD equations are implemented in the code in a conservative form, given by

$$\partial_t \rho \ + \ \nabla \cdot (\rho \mathbf{v}) = 0 \tag{7}$$

$$\partial_t (\rho \mathbf{v}) \ + \ \nabla \cdot [\rho \mathbf{v}\mathbf{v} - \mathbf{B}\mathbf{B} + p_{\rm t}\mathbf{I}] = 0 \tag{8}$$

$$\partial_t \mathbf{B} \ + \ \nabla \cdot (\mathbf{v}\mathbf{B} - \mathbf{B}\mathbf{v}) = 0 \tag{9}$$

where ρ is the mass density, $\mathbf{v}$ is the velocity and $\mathbf{B}$ the magnetic field. The total pressure is written as $p_{\rm t} = p + \mathbf{B}^2/2$ and $\mathbf{I}$ is a unit tensor.

We use the simple isothermal equation of state, where the pressure is given by $p = \rho c_s^2$, and the sound speed is set to a small value of $c_{\rm s} = 10^{-3} v_{\rm A}$ to only have negligible compressive effects in the evolution. Viscous and resistive dissipation effects are explicitly added as parabolic terms on the right-hand side of the conservation equations to control the non-idealness of the evolution in relation to numeric dissipation. We always choose the viscosity ν to be equal to the resistivity η and uniform across the domain. The time-evolution is implemented as second-order Runge-Kutta time-stepping and we use the Roe type Riemann solver to minimize numeric dissipation. The divergence free constraint of the magnetic field is maintained by the divergence cleaning method (Dedner *et al.*, 2002). We checked for various times during the evolution that the method is successful in keeping the divergence error equal or below 1 percent of the current magnitude.

To keep numeric diffusivity small against the explicit dissipation terms, a sufficiently high grid resolution is needed in the vicinity of the strong current layers. To achieve this feat with limited computational resources, we make use of the stretched grid features of PLUTO. We decompose the domain in the transverse x and y directions into three subdomains. From -1 to -0.1 we have a stretched grid of decreasing cell size, matching to the uniform grid from -0.1 to 0.1 in the sheet region. From 0.1 to 1 the cell size increases again. Each of the outer subdomains is covered by 50 grid points, while we have up to 400 points in the centre region, giving a maximum resolution (or grid-cell size) of $d = 5 \times 10^{-4}$, which we use for runs with the smallest resistivities. The resolution in z direction is kept constant at 100 points, assuming that the relevant dynamic scales are only perpendicular to the z-axis. We confirmed the soundness of our grid approximation with comparison runs between uniform grids and the described stretched patch grid. We found the differences in field and current magnitudes to be smaller than a few percent, and the qualitative field evolution

was practically indistinguishable, encouraging our confidence in the choice for the grid setup.

References

Aulanier, G., Pariat, E., Démoulin, P.: 2005, Current sheet formation in quasi-separatrix layers and hyperbolic flux tubes. *Astron. Astrophys.* **444**, 961. DOI. ADS.

Aulanier, G., Pariat, E., Démoulin, P., DeVore, C.R.: 2006, Slip-running reconnection in quasi-separatrix layers. *Solar Phys.* **238**, 347. DOI. ADS.

Baker, D., van Driel-Gesztelyi, L., Mandrini, C.H., Démoulin, P., Murray, M.J.: 2009, Magnetic reconnection along quasi-separatrix layers as a driver of ubiquitous active region outflows. *Astrophys. J.* **705**, 926. DOI. ADS.

Biskamp, D.: 1986, Magnetic reconnection via current sheets. *Phys. Fluids* **29**, 1520. DOI. ADS.

Craig, I.J.D., Effenberger, F.: 2014, Current singularities at quasi-separatrix layers and three-dimensional magnetic nulls. *Astrophys. J.* **795**, 129. DOI. ADS.

Craig, I.J.D., Fabling, R.B.: 1996, Exact solutions for steady state, spine, and fan magnetic reconnection. *Astrophys. J.* **462**, 969. DOI. ADS.

Craig, I.J.D., Litvinenko, Y.E.: 2005, Current singularities in planar magnetic X points of finite compressibility. *Phys. Plasmas* **12**, 032301. DOI. ADS.

Craig, I.J.D., McClymont, A.N.: 1993, Linear theory of fast reconnection at an X-type neutral point. *Astrophys. J.* **405**, 207. DOI. ADS.

Craig, I.J.D., Pontin, D.I.: 2014, Current singularities in line-tied three-dimensional magnetic fields. *Astrophys. J.* **788**, 177. DOI. ADS.

Craig, I.J.D., Sneyd, A.D.: 1986, A dynamic relaxation technique for determining the structure and stability of coronal magnetic fields. *Astrophys. J.* **311**, 451. DOI. ADS.

Dedner, A., Kemm, F., Kröner, D., Munz, C.-D., Schnitzer, T., Wesenberg, M.: 2002, Hyperbolic divergence cleaning for the MHD equations. *J. Comput. Phys.* **175**, 645. DOI. ADS.

Demoulin, P., Henoux, J.C., Priest, E.R., Mandrini, C.H.: 1996, Quasi-Separatrix layers in solar flares. I. Method. *Astron. Astrophys.* **308**, 643. ADS.

Effenberger, F., Thust, K., Arnold, L., Grauer, R., Dreher, J.: 2011, Numerical simulation of current sheet formation in a quasiseparatrix layer using adaptive mesh refinement. *Phys. Plasmas* **18**, 032902. DOI. ADS.

Finn, J.M., Billey, Z., Daughton, W., Zweibel, E.: 2014, Quasi-separatrix layer reconnection for nonlinear line-tied collisionless tearing modes. *Plasma Phys. Control. Fusion* **56**, 064013. DOI. ADS.

Forbes, T.G.: 1982, Implosion of a uniform current sheet in a low-beta plasma. *J. Plasma Phys.* **27**, 491. DOI. ADS.

Galsgaard, K.: 2000, Dynamical investigation of three-dimensional reconnection in quasi-separatrix layers in a boundary-driven magnetic field. *J. Geophys. Res.* **105**, 5119. DOI. ADS.

Heerikhuisen, J., Craig, I.J.D.: 2004, Magnetic reconnection in three dimensions - Spine, fan and separator solutions. *Solar Phys.* **222**, 95. DOI. ADS.

Heerikhuisen, J., Litvinenko, Y.E., Craig, I.J.D.: 2002, Proton acceleration in analytic reconnecting current sheets. *Astrophys. J.* **566**, 512. DOI. ADS.

Longcope, D.W.: 2005, Topological methods for the analysis of solar magnetic fields. *Living Rev.Solar Phys.* **2**, 7. DOI. ADS.

McClymont, A.N., Craig, I.J.D.: 1996, Dynamical finite-amplitude magnetic reconnection at an X-type neutral point. *Astrophys. J.* **466**, 487. DOI. ADS.

Mignone, A., Bodo, G., Massaglia, S., Matsakos, T., Tesileanu, O., Zanni, C., Ferrari, A.: 2007, PLUTO: A numerical code for computational astrophysics. *Astrophys. J. Suppl.* **170**, 228. DOI. ADS.

Mignone, A., Zanni, C., Tzeferacos, P., van Straalen, B., Colella, P., Bodo, G.: 2012, The PLUTO code for adaptive mesh computations in astrophysical fluid dynamics. *Astrophys. J. Suppl.* **198**, 7. DOI. ADS.

Milano, L.J., Dmitruk, P., Mandrini, C.H., Gómez, D.O., Démoulin, P.: 1999, Quasi-separatrix layers in a reduced magnetohydrodynamic model of a coronal loop. *Astrophys. J.* **521**, 889. DOI. ADS.

Pontin, D.I., Craig, I.J.D.: 2005, Current singularities at finitely compressible three-dimensional magnetic null points. *Phys. Plasmas* **12**, 072112. DOI. ADS.

Pontin, D.I., Bhattacharjee, A., Galsgaard, K.: 2007, Current sheets at three-dimensional magnetic nulls: Effect of compressibility. *Phys. Plasmas* **14**, 052109. DOI. ADS.

Pontin, D.I., Hornig, G., Wilmot-Smith, A.L., Craig, I.J.D.: 2009, Lagrangian relaxation schemes for calculating force-free magnetic fields, and their limitations. *Astrophys. J.* **700**, 1449. DOI. ADS.

Priest, E., Forbes, T.: 2000, *Magnetic Reconnection*, Cambridge University Press, Cambridge, Chapter 7. ADS.

Priest, E.R., Titov, V.S.: 1996, Magnetic reconnection at three-dimensional null points. *Phil. Trans. Roy. Soc. London* **354**, 2951. DOI. ADS.

Rickard, G.J., Titov, V.S.: 1996, Current accumulation at a three-dimensional magnetic null. *Astrophys. J.* **472**, 840. DOI. ADS.

Stanier, A., Browning, P., Dalla, S.: 2012, Solar particle acceleration at reconnecting 3D null points. *Astron. Astrophys.* **542**, A47. DOI. ADS.

Titov, V.S.: 2007, Generalized squashing factors for covariant description of magnetic connectivity in the solar corona. *Astrophys. J.* **660**, 863. DOI. ADS.